COATING SHRINKAGE DURING EVAPORATION: observation, measurement and modelling within a network structure

G.M. Laudone*, G.P. Matthews*[§] and P.A.C. Gane**

**Environmental and Fluid Modelling Group, University of Plymouth,*

Plymouth PL4 8AA, UK.

*** Omya AG, CH-4665 Oftringen, Switzerland.*

[§] To whom correspondence should be addressed. Email: pmatthews@plymouth.ac.uk

ABSTRACT

Coating shrinkage upon drying is a phenomenon well known to the paper coating industry where it often causes changes in the final structure of the coating layer, leading to poor results in terms of gloss, light scattering, surface strength, coverage and printability. The aim of this paper is to improve the understanding of coating shrinkage by measuring the forces related to the capillarity, acting at the free liquid front, in combination with the flocculation, film forming and compressibility characteristics of the coating structure and binders.

Shrinkage while the coating layer dries has been successfully measured by observing the deflection of coated strips of a dimensionally stable synthetic substrate. Ground calcium carbonate was used as the coating pigment together with latex binders of low and high T_g latex, respectively, and using starch additionally as an example of a natural film-forming binder. The final dry coatings were analysed with mercury porosimetry and by scanning electron microscopy in order to characterise their porous structure.

The mercury intrusion curves were analysed with Pore-Cor, a software package that is able to generate a three-dimensional network structure representative of the porous medium. The simulated structures were compared with the microscope images and provided evidence of the drying behaviour of the different components of paper coating and their influence on the final structures of the dry coating layer. The shrinking behaviour of coating colour formulations, which has usually been interpreted as shrinkage of the polymer upon film-forming, has been explained in terms of surface capillary forces acting on the packing structure of the coating at the first critical concentration. The structures undergoing shrinkage are shown to be affected by the degree of flocculation within the coating, which depends on the nature of the binder used.

Keywords: Paper coating, binder film formation, shrinkage, drying of porous structures, capillary force, pore-level properties.

INTRODUCTION

Binders are used in the paper coating industry in order to provide good cohesion of the porous structure formed by mineral pigments, such as clay, talc or calcium carbonate, and adhesion of the coating to the substrate. They can be grouped into two main categories:

- natural, like starches or proteins;
- synthetic, like styrene-butadiene, styrene-acrylic latex or polyvinyl acetate.

A typical coating colour suitable for offset printing consists, on a dry basis, of mineral pigment particles, with 10-20 w/w% of binder based on 100 w/w% of pigment. The coating colour is applied to the base as a slurry with 50-70 w/w% of solid content and is usually dried thermally using infra red and hot air dryers. Other compounds, such as dispersants, are used in lower percentages to act as stabilisers and to make the components compatible in water suspensions.

The use of natural binders in coating colour formulations often leads to poor results in terms of optical and printing properties, assumed due partly to shrinkage of the coating layer upon drying. Synthetic binders suffer less from this problem.

Previous attempts have been made to study the consolidation of the coating layer during drying, both experimentally [1,2], and using models [3,4,5]. All these studies use the description of Watanabe and Lepoutre

[1], in which the drying process is divided into three phases, separated by two critical concentrations. The initial application of the coating layer is thus followed by a first phase of water evaporation at the liquid-air interface. This phase is unaffected by the solid content suspended in the liquid phase as the liquid is in excess and the surface is defined by free liquid. At the *first critical concentration* (FCC), a three-dimensional network is formed and particle motion is greatly restricted. The water-air interfaces recede into the surface pores forming capillary elements, creating a differential Laplace pressure that contributes to a shrinkage of the network. This continues until the *second critical concentration* (SCC) is reached, at which the network is fixed and air enters the rigid structure as the liquid retreats.

Despite the previous investigations, the measurement of the surface forces acting upon drying has not been attempted before and the great difference in final properties for natural and synthetic latex binder-based coating colours has not been clearly explained. By combining a new experimental technique for the measurement of surface forces with a newly developed software package, it has been possible to reach a better understanding of the drying process. In particular, we explain the physical cause of the high coating shrinkage observed when typical natural binding systems are used in the coating colour formulation.

In our study, we simplify the process by using an impermeable dimensionally stable substrate. In commercial paper coating applications, the absorbency of the base sheet is a dominant factor. Superposed on this is the evaporation phenomenon during drying. We simulate here the evaporation process during evaporative drying, but not the role of base sheet absorbency.

EXPERIMENTAL

Method and Materials

Due to the complexity and the small dimension of the system in the out of plane direction, the measurement of the forces acting upon drying could not be carried out with any direct force-measurement method. These forces were therefore measured by observing how an elastic material reacts to them. A series of tests on several polymeric materials led to the choice of Synteape as substrate for our experiments (a product of Arjo Wiggins Limited). It consists of a synthetic laminate substrate made of stretched polypropylene sheets filled with calcium carbonate. Its slightly rough surface, which enables the adhesion of the coating colour, makes it a useful substrate in the study of paper coating in isolation from fibrous base sheets. Together with its elasticity, this property makes it the ideal substrate for our experiments. Furthermore, the forces could not be calculated from the application of coating colours to a natural base paper, due to its unstable behaviour; under the initial high moisture conditions of drying, its fibres are free to rearrange, thus preventing any measurable deformation. However, as the coating dries, the fibres stop rearranging, and there is a resulting non-uniformity of the coating caused by the combined shrinkage of the coating and the base paper.

Each coating colour was applied to a strip of the synthetic base, and the deflection of the strip upon drying was measured as a function of weight loss during evaporation at ambient conditions. The standard mechanical beam theory was then used to calculate, through the Young's modulus of the substrate, the forces acting on the substrate's surface, causing such a deflection.

The Elementary Beam Theory approach for the measurement of shrinkage forces is novel in the paper coating field, but a similar approach was used by Perera [6] for the measurement of shrinkage forces in a paint film upon drying. Perera showed the effect of the glass transition temperature of the binding system and of the critical pigment volume concentration (cPVC) on the stress measured while the coating layer dries. The critical pigment volume concentration in that work was the value of pigment concentration below which all the voids of the structure had been filled with binder, forming a non-porous paint film.

The substrate strips used in our experiments were 4.5 cm long, 0.5 cm wide and 0.01 cm thick. These dimensions formed the designated coordinates x, y and z respectively. The weights of the strips were considered negligible when compared with the forces acting to cause the deflection of the beam.

The mechanical properties of the substrate-coating colour system were assumed to be constant during the drying of the coating layer. This is an approximation as the coating structure develops some mechanical resistance as it changes from the FCC to the SCC, i.e. the coating layer changes its mechanical properties upon drying, from plastic, through viscoelastic to a brittle structure. However, the exact mechanical transitions between these states of the coating are not the target of investigation, rather the roles of the various force components as a function of time and solid concentration which lead to the transitions. Furthermore, the shrinkage forces which drive this change must, by definition, be greater than the physical resistance to change. The coating layer was therefore assumed to act only as a *stress deliverer*, whilst itself having little or no stress growth as a direct result of the

resulting bending strain. The internal stress of the coating layer is released in the *x* direction causing the sample to curl, as shown in Fig.1. Curling in the *y* direction also occurs, but as the sample is narrow, this has a much smaller measurable effect, which in turn is not monitored.

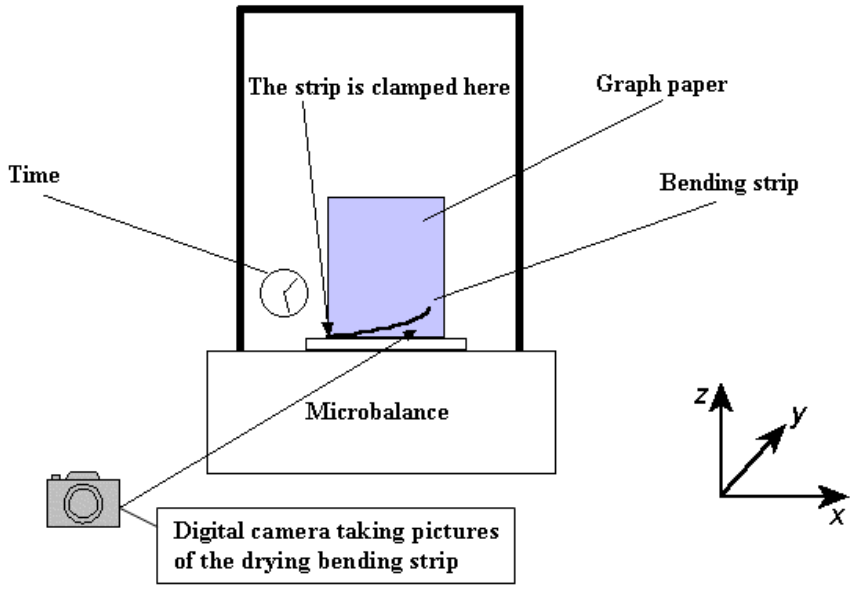

Figure 1 - Diagram of the experimental apparatus, viewing in the *xz* plane as shown.

The experimental apparatus, presented in Fig.1, was designed and built in order to take pictures of the sample deflection during the drying process whilst measuring its weight loss, making it possible to find the forces acting on the surface of the substrate as a function of % weight (water) loss. It consists of a microbalance, connected to a computer which acquires and stores the weight of our samples while the drying occurs. The basis for this microbalance method is described by Schoelkopf et al. [7]. The coated strips were clamped to the sample plate of the microbalance and the chamber above the plate was closed, in order to avoid external disturbances of the evaporation and weighing process.

Coating Colour Formulations

The mineral pigment used in our experiments reported here was ground calcium carbonate (GCC). Clay platelets, together with their tendency to adsorb starch [8], give rise to highly anisotropic porous structures, in which the particle orientations can play a very important but difficult to define role. Their use has therefore been avoided. Similarly, the use of precipitated calcium carbonate (PCC) in its aragonitic form can lead to similar anisotropy problems, while calcitic forms of PCC have a very narrow particle size distribution, which leads to highly permeable structures, which in turn would reduce the capillary effect which we wish to observe. Therefore, Hydrocarb 90 OG, a dispersed broad size distribution GCC limestone from Orgon, France, with 90 w/w% of particles having an equivalent spherical diameter < 2 µm, has been chosen for the preparation of our samples (Hydrocarb is a product name of Omya AG, CH 4665 Oftringen, Switzerland).

In order to reach an understanding of the influence of binder systems on the drying process, coating colours were prepared using both natural and synthetic binders:

- thermally modified maize starch C-film 07321 (C-film is a product name of Cerestar, France);
- high glass transition temperature (T_g = 23 °C) acrylic latex Acronal S320D (Acronal is a product name of BASF, Ludwigshafen, Germany) and
- low T_g (5 °C) styrene-butadiene latex DL930 (DL930 is a product name of Dow Chemical, Midland, USA).

The minimum film-forming temperatures for the latex binding systems are given by manufacturers as 1 °C above T_g, i.e. 24 °C and 6 °C respectively. Their different chemical structure, especially the serum phase, has been considered as only a minor but perhaps discernable factor in our experiments since both latices are designed for stability in the presence of calcium ions, widely used in the paper coating industry and they are not “self-

thickening".

The coating colours used in the preparation of our coated samples had a solids content of about 55 w/w%. On a dry basis, the composition of our coating colours was 25 w/w% binder and 75 w/w% pigment. This is a higher percentage of binder than in a typical industrial paper coating colour, but the level is chosen in order to maximise the effect of any binder-related shrinkage in the following observations. A preliminary set of experiments has shown that the effect of binder is proportional to its content within the dosage range above the cPVC, and so the increased binder quantity is a useful experimental parameter to apply without influencing the basic mechanisms themselves. This is confirmed by Groves and Lanham [9], who investigated the gloss variation and volumetric shrinkage for latex-clay coatings. They measured a minimum value of gloss for coating colours containing 30 w/w% and a maximum volumetric shrinkage for 35 w/w% of latex in the coating formulations. These measurements show that the critical pigment concentration for the coating used in their experiments is 65-70 w/w% corresponding to more than 50% in volume of latex in the coating colour formulation. Their measurement showed proportionality between latex content and volumetric shrinkage above the cPVC, while the shrinkage was constant below the cPVC.

The samples used in our experiments have pigment content above the critical pigment volume concentration for the particular latex-$CaCO_3$ mixtures, as confirmed below by the results of the mercury porosimetry intrusion curves and scanning electron microscopy imaging of the samples, confirming the presence of a void structure.

The pH of the coating colours was corrected to 9 by adding NaOH.

The viscosity values of the $CaCO_3$-latex coating colours, used in the preparation of our samples, were measured by using a Brookfield viscometer at 20, 50 and 100 rpm. The results are presented in Fig.2. The suspension containing low T_g latex has a viscosity some 3 times higher than that containing the high T_g latex. This viscosity difference is probably due to the interaction between soluble species in the latex-pigment mix affecting either the pigment adsorption properties or stability of the latex against flocculation or both [10]. This may mean that the colour is more flocculated in the case of the low T_g latex formulation. No additional thickener or water retention aid was added. Thickeners act in general to flocculate the coating colour. To study the effect of binders on shrinkage in isolation, such thickeners were purposefully omitted. Furthermore, the solid content of the coating colours will increase as evaporation takes place, and thus the elasticity will increase. We can assume that the viscosity differences at low solids have less effect on the drying forces than the structural and menisci parameters at high solids, although the precursor low solids structural properties may in turn affect the high solids structures.

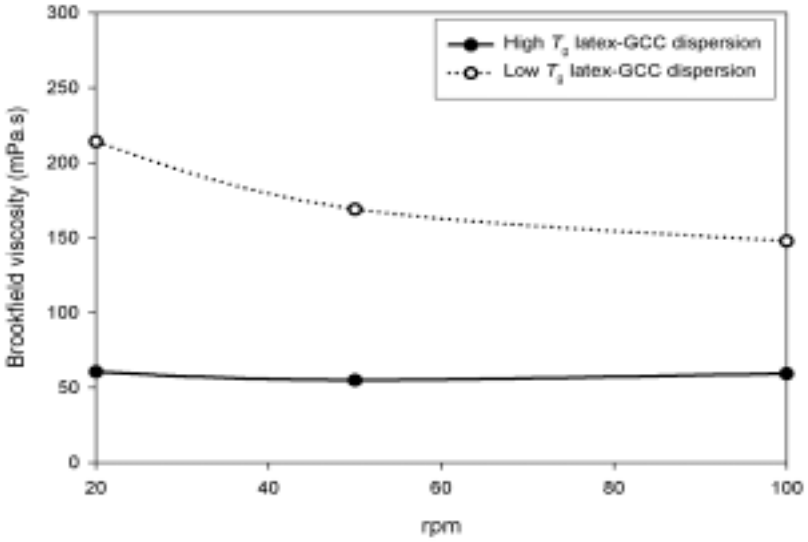

Figure 2 – Viscosity values of the latex-GCC dispersions used in the preparation of the samples. Both the coating colours show a relatively low viscosity, compared with the starch formulation (> 1 000 mPas), although the low T_g sbr latex formulation shows some indication of slight structure formation.

In order to investigate the effect of the amount of coating colour applied, and thus of the thickness of the coating layer, the strips were coated using two different draw-down coating rods. The rods were labelled "rod 2"

(applying about 10 gm^{-2} of dry coating corresponding to a dry coating layer thickness of about 5 μm) and "rod 3" (applying about 20 gm^{-2} of dry coating, corresponding to a dry coating layer thickness of about 10 μm).

Control samples consisted of pure GCC slurry without added binder, as well as applied pure binder layers in the absence of pigment.

Sample Characterisation

The porous structures of the dried coatings were analysed with a Micromeritics Autopore III mercury intrusion porosimeter, which makes it possible to determine the pore size distribution of porous materials measuring the mercury intrusion for increasing applied pressures, up to 414 MPa. Such a technique can be also applied to porous materials supported on laminated substrates, like in these experiments, or fibrous substrates, such as paper [11].

In order to avoid the complication of intrusion of mercury into the laminated structure of the elastic substrate used for the bending strips experiment, non-porous aluminium foil was coated, in parallel, with the same coating colour formulations as used in the bending experiments, dried in the same conditions and the resulting dry coating layer analysed by mercury porosimetry.

The surfaces of the dry samples were examined under scanning electron microscopy (Figs. 3-8 where the scale bar is 5 μm). Commentary on the observations is made in the relevant figure captions.

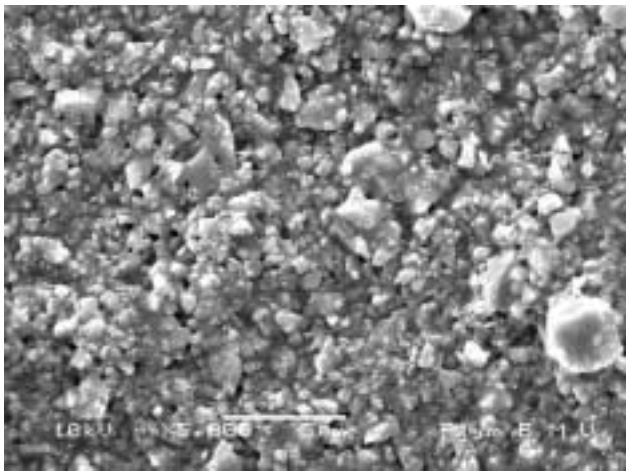

Figure 3 - Micrograph of a low T_g latex-based coating applied with rod 2 - showing the restraining action of large particles in a thin low coat weight layer.

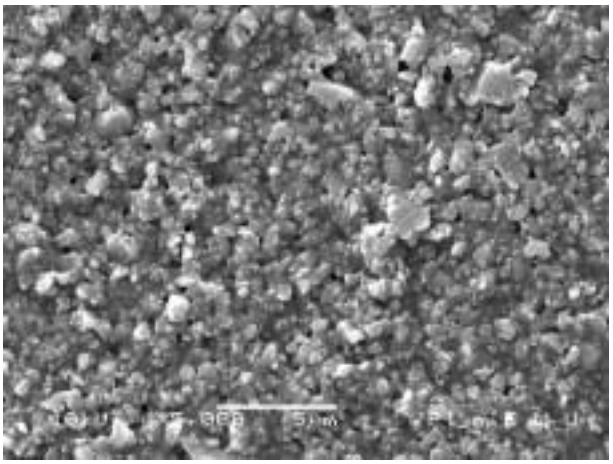

Figure 4 - Micrograph of a low T_g latex-based coating applied with rod 3 - now that the coating is thicker, the particles are more free to move, the filming latex then holds the shrunken structure in place**.**

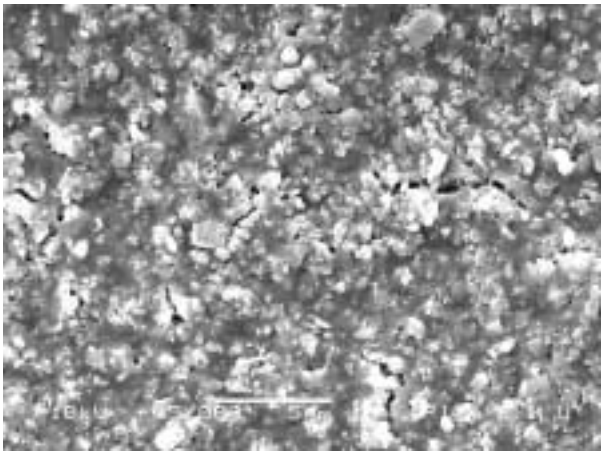

Figure 5 - Micrograph of a high T_g latex-based coating applied with rod 2 - note the cracks beginning to form as a relief of stress within the rigid structure provided by the high T_g latex.

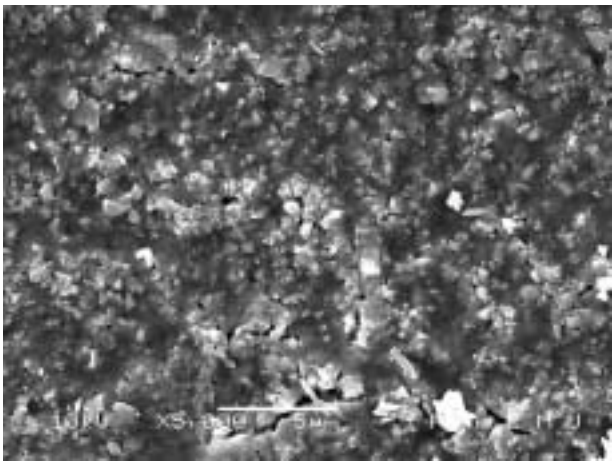

Figure 6 - Micrograph of a high T_g latex-based coating applied with rod 3 – under high resolution, it can be seen that the cracks here go deep into the coating structure.

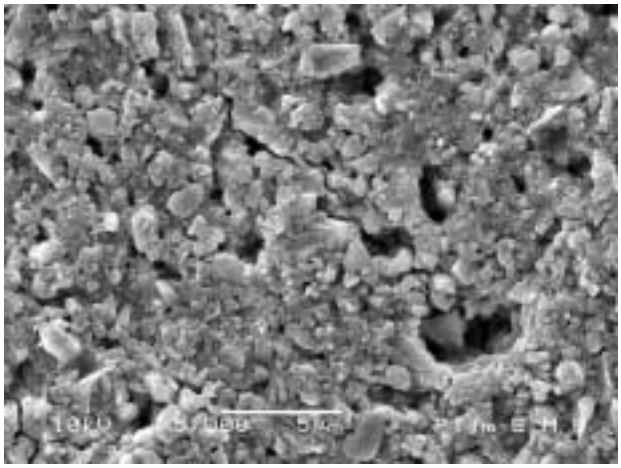

Figure 7 - Micrograph of starch-based coating applied with rod 2 - note the large size of the floc-structured particles leaving large voids between them. The large size of the flocs is a serious constraint to rearrangement at light coat weight application on this substrate.

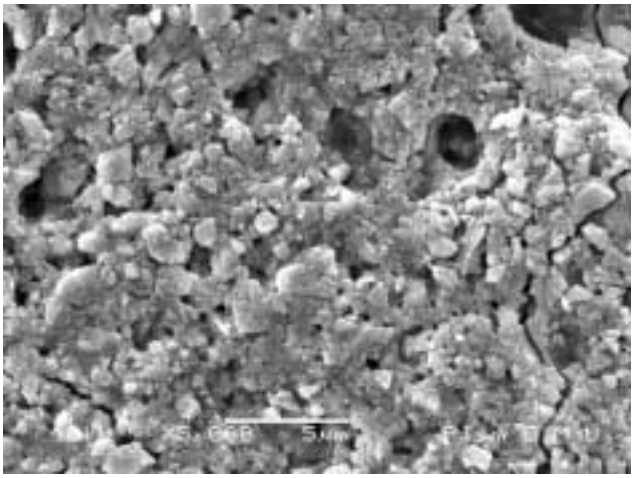

Figure 8 - Micrograph of a starch-based coating applied with rod 3 - the thicker coating allows more rearrangement and more consolidation, itself leading to greater shrinkage stress.

Modelling Software

The mercury porosimetry intrusion curves for the dry samples were studied with the aid of newly developed software packages.

Pore-Comp calculates correction factors on the mercury porosimetry intrusion curves for the compressibility of the mercury, the expansion of the chamber containing the samples and the compressibility of the skeletal solid phase of the sample at high pressures. It is based on the equation from Gane et al. [12] (see www.pore-cor.com):

$$V_{\text{int}} = V_{\text{obs}} - \delta V_{\text{blank}} + \left[0.175 (V^1_{\text{bulk}}) \log_{10} \left(1 + \frac{P}{1820} \right) \right] - V^1_{\text{bulk}} (1 - \Phi^1) \left(1 - \exp \left[\frac{(P^1 - P)}{M_{\text{ss}}} \right] \right) \quad (1)$$

where V_{int} is the volume of intrusion into the sample, V_{obs} the intruded mercury volume reading, δV_{blank} the change in the blank run volume reading, V^1_{bulk} the sample bulk volume at atmospheric pressure, P the applied pressure, Φ^1 the porosity at atmospheric pressure, P^1 the atmospheric pressure and M_{ss} the bulk modulus of the solid skeletal material.

The corrected mercury porosimetry intrusion curves can be used as input data for the Pore-Cor software package [13,14], which can simulate the pore-level properties of porous media (Pore-Cor is a software name of the Environmental and Fluid Modelling Group, University of Plymouth, UK). It generates three-dimensional network structures made of 1 000 cubic pores connected by cylindrical throats and equally spaced in a repeated unit cell. The simulation was performed by optimising a set of four parameters (connectivity, pore-skew, throat-skew and correlation level) to match the experimentally measured porosity and percolation characteristics, as measured by mercury porosimetry. The connectivity represents the average number of throats connected to each pore, between 0 and 6. The software package is able to simulate both completely random structures and correlated ones. The correlation level is a parameter with value between 0 and 1 and represents the level of ordering of the structure: the more the structure is ordered (vertically or horizontally banded), the more the value of the correlation level tends to 1. A correlation level equal or close to 0 represents a random structure [15]. It is also possible to generate anisotropic structures [16]. The throat skew is the percentage number of throats of the smallest size. The pore skew is a scaling factor, which increases the sizes of the pores by a constant value.

This approach created simulated pore structures with different best-fit values of the adjustable parameters, all of which matched the experimental properties. To cope with this, the model creates different families of structures known as “stochastic generations”. Each stochastic generation is created by using a different set of pseudo-random starting numbers. If the unit cell is the same size as the Representative Elementary Volume (REV) of the sample, and its complexity is equivalent to the complexity of the experimental void structure, then different stochastic generations will all have the same properties, as the random effects will average out across the unit cell. Usually, however, the model does not fulfil the criteria of representing the REV of the sample, and the variability of the results for different stochastic generations must be analysed statistically.

The simulated structures can be used to calculate pore-level properties such as gas and fluid permeability [15], tortuosity [17], particle size distribution, throat and pore size distributions and dynamic liquid absorption [18,19]. The software provides also a Virtual Reality environment in which the simulated structures can be visualised and local effects such as menisci positions and preferred pathways for wetting fluids [20] can be identified and observed.

BENDING EXPERIMENTS

All experiments were carried out at 20 °C ± 1 °C, and ambient humidity. It was not necessary to control the humidity, as we measured the extent of bending as a function of solids rather than the absolute rate of bending and the timescale was assumed long enough to allow for diffusional processes to occur.

A first series of experiments was carried out in order to find out the stiffness of the beam, *EI*, with *E* representing the Young's modulus and *I* the second moment of inertia, for the strips of elastic substrate, as previously discussed. The weight of the strips was negligible when compared to the forces acting on the surface upon drying of a coating layer but enough to cause a small deflection. This deflection was measured and used to calculate the value of *EI*.

Experiments were then carried out to measure the curling of all the samples during drying. The bending of the strips was measured in the *xz* plane (the same view as in Fig.1) and the data collected from the microbalance.

STRESS RESULTS

The control samples coated with calcium carbonate slurry only made with the use of rod 2, i.e. low coating weight applied, showed a deflection and a subsequent relaxation that were too small and rapid to be recorded and studied with the photographic technique in use. Control samples coated with higher coating weight (rod 3, calcium carbonate only) did, however, permit recorded observation. These samples bend as soon as the drying begins and the water recedes into the porous structure created by the particles of calcium carbonate, reaching a peak of about 50-60 Pa, as shown in Fig.9. In Figs. 9-12 the % weight loss represents the percentage of the samples' loss of weight upon drying due to water evaporation. However, as more water leaves, the total effect of the capillary forces reduces again, confirming the isotropic relaxation of the non-bound particulate structure. This ultimately leads to a complete relaxation of the sample with no stress retention at all. These data for calcium carbonate alone made possible a comparison of the drying behaviours induced by the presence of the different types of binders.

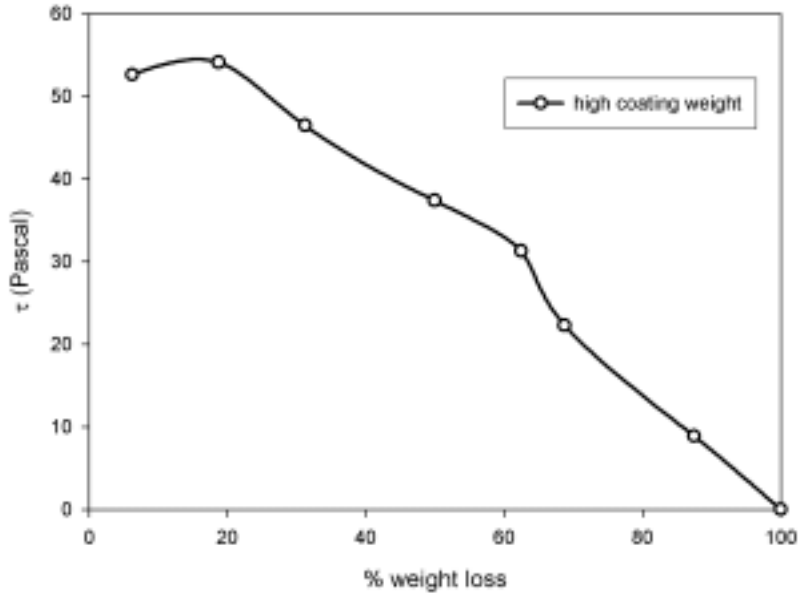

Figure 9 - Stress acting on samples coated with slurry of calcium carbonate only.

The measurement of the stress acting on the surface of the coated strips when containing a high T_g latex leads to the interesting results shown in Fig.10. It can be seen that the maximum τ (= 11 Pa) was much less than for the pigment only samples. Once again, the relaxation is observed as the menisci retreat during drying, and very little difference is observed between low and high coat weight.

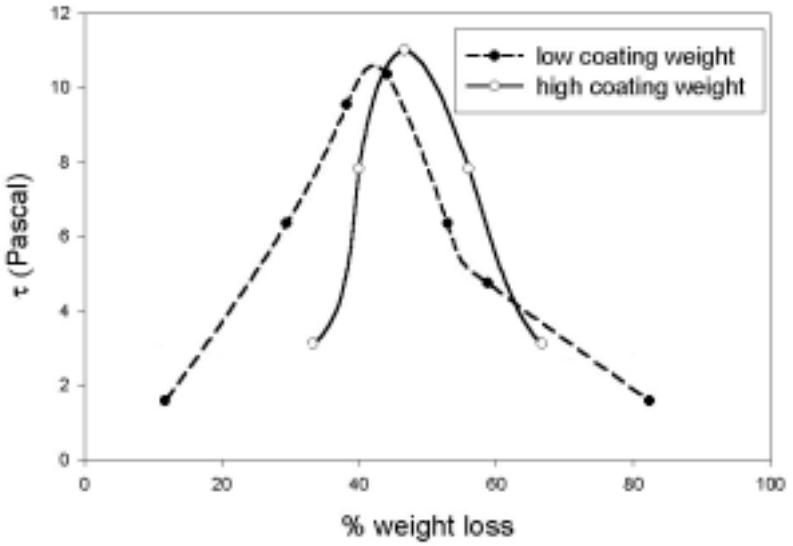

Figure 10 - Stress acting on samples coated with a high T_g latex-based coating colour.

The low T_g latex-based coating colour reproduced the above mentioned higher values of stress acting on the surface of the drying sample (Fig.11). However, the deformation, unlike the cases for $CaCO_3$ alone or with high T_g latex, was in this case not completely reversible as the water left the structure. The strip was still bent when dry and did not entirely relax. The effect of coat weight is clearly seen, in which the low coat weight constraints on particle motion due to particle size limit the stress development.

The results of stress measurement for latex-based coating colours show good agreement with the trends presented by Perera [6] for pigment concentration above the cPVC in presence, respectively, of a good or poor coalescent.

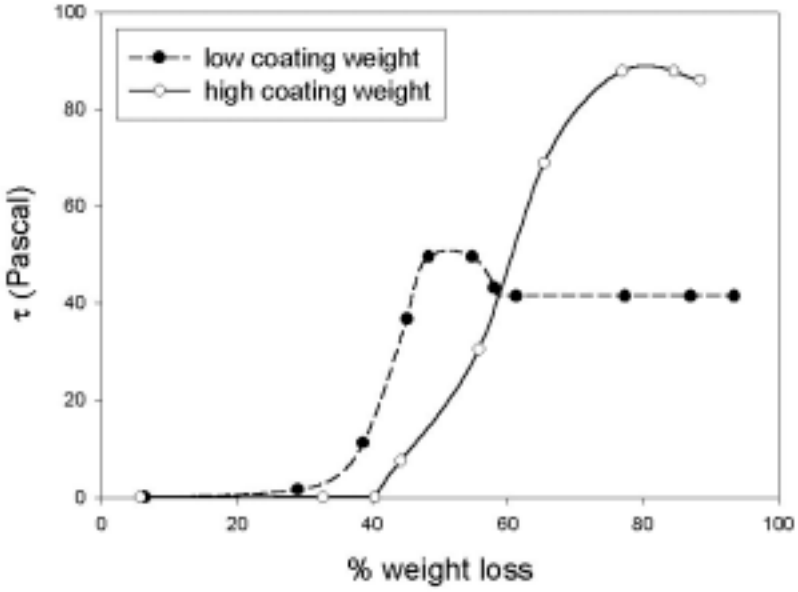

Figure 11 - Stress acting on samples coated with a low T_g latex-based coating colour.

Fig. 12 shows τ measured upon drying of starch-based coating colours. It is clear that the forces acting on the surface of the substrate while the coating layer is drying are far larger when starch is used as binding system. The increase in stress τ with % weight loss is much steeper for the starch-containing samples than for the latex coatings and this seems to suggest at first sight that the starch itself is forcing the structure to shrink, i.e. the traditional interpretation. Here we note the even larger difference between low and high coat weight.

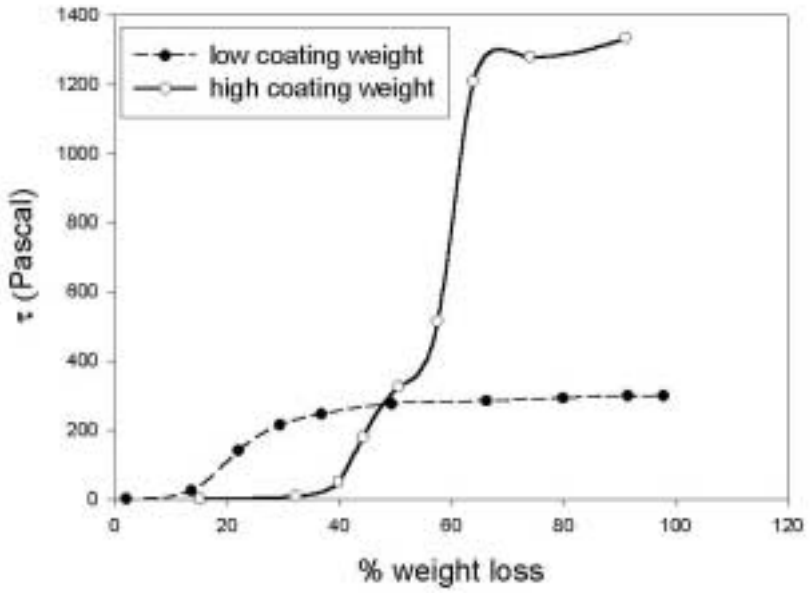

Figure 12 - Stress acting on samples coated with a starch-based coating colour, illustrating the effect of particle or floc size in relation to layer thickness on the shrinkage phenomena within a thin layer structure.

MODELLING OF MERCURY INTRUSION

Samples prepared using the coating colour formulations described above and dried under the same conditions as for shrinkage testing were applied, as previously described, on a non-porous aluminium foil substrate and analysed using mercury intrusion porosimetry. The results were corrected using the software already described in order to take into account compressibility of mercury and compressibility of the samples themselves. All the mercury intrusion curves showed a bimodality with a rather atypical mercury intrusion for pore diameters in the order of 2-10 μm, and, in the case of low T_g latex and starch, higher values of porosity for higher coating weight applied.

In the paper coating industry it is well known [21] that the higher the coat weight, the lower the light scattering, which implies loss of interparticle porosity and reduction of layer thickness per unit weight of coating, i.e. densification. The anomalous trends in the porosity for low T_g latex and starch-based coating colours could be explained with the appearance of surface cracks with size in the order of magnitude of micrometres. This "pore size" measured by the porosimeter associated with surface cracks lies outside the light scattering pore size and outside the pore size range that affects interparticle absorption, i.e. they are really discontinuities and therefore do not describe the compacted coating regions which have undergone shrinkage. An attempt to fit these bimodal mercury intrusion curves with the network simulation software was carried out and led to a series of horizontally banded structures with large surface throats, which is the only way the software could model such surface cracking.

The bimodal intrusion curves were, therefore, divided into two different distribution curves, one for the coarse range of “pore-size” (cracking) and one for the finer range (the coating having undergone shrinkage). The finer pore-size distribution curves were scaled to represent the region of interest, so that the intrusion measurements started from zero at the beginning of this range, and this led to the intrusion curves shown in Fig.13.

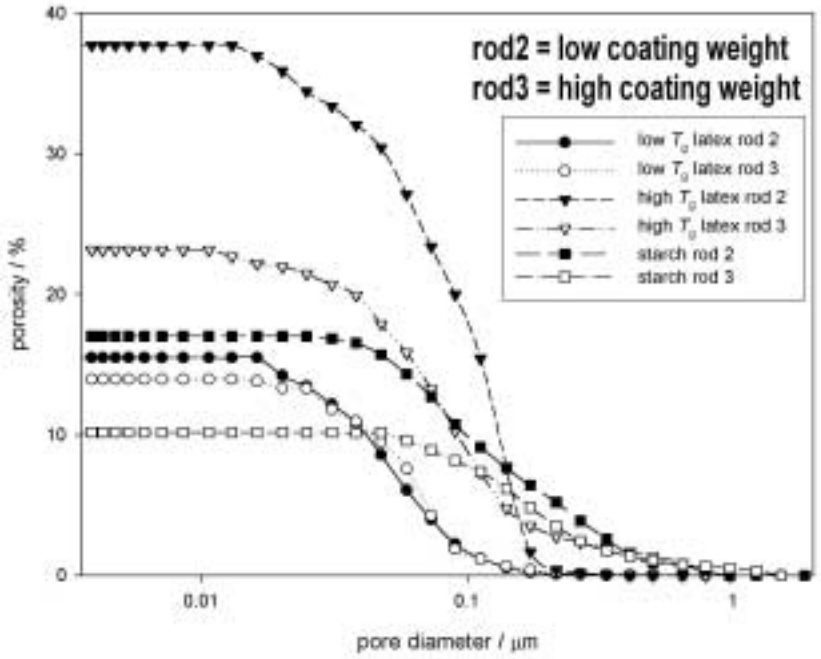

Figure 13 - Mercury porosimetry intrusion curves - comparing these intrusion curves with the micrographs in Figs. 3-8 give good correlation in respect to the pore structure developed in the regions between the cracks**.**

The newly defined mercury intrusion curves described above were used as input data for the network simulator. For each sample, 10 different "stochastic generations" were used and Paired Student *t*-tests were performed on the mean values of each of the fitting parameters, and on the values of the liquid permeability of the modelled coating layers in order to determine if there were any significant differences in their values. The results of the software simulation are presented in Table 1.

Table 1 – results of the software modelling

Sample	Experimental and simulated porosity / %	Simulated connectivity	Simulated correlation level	Simulated throat skew	Simulated pore skew	Simulated network liquid permeability / µDarcy
Low T_g latex rod 2	15.50	4.96	0.16	2.24	4.47	9.47E-06
Low T_g latex rod 3	13.96	5.08	0.17	2.15	3.06	8.49E-06
High T_g latex rod 2	37.72	5.36	0.24	1.84	3.34	4.75E-04
High T_g latex rod 3	23.15	4.01	0.29	1.31	3.61	2.07E-04
Starch rod 2	17.01	4.16	0.25	1.26	3.47	1.97E-04
Starch rod 3	10.17	5.04	0.22	1.36	2.36	1.15E-04

Examples of the simulated 3D structures generated by the software model are shown in Figs.14-19. Although the simulated void structures are a gross simplification of those actually existing in the real samples, they nevertheless reveal some interesting and fundamental properties which are highlighted in the captions below.

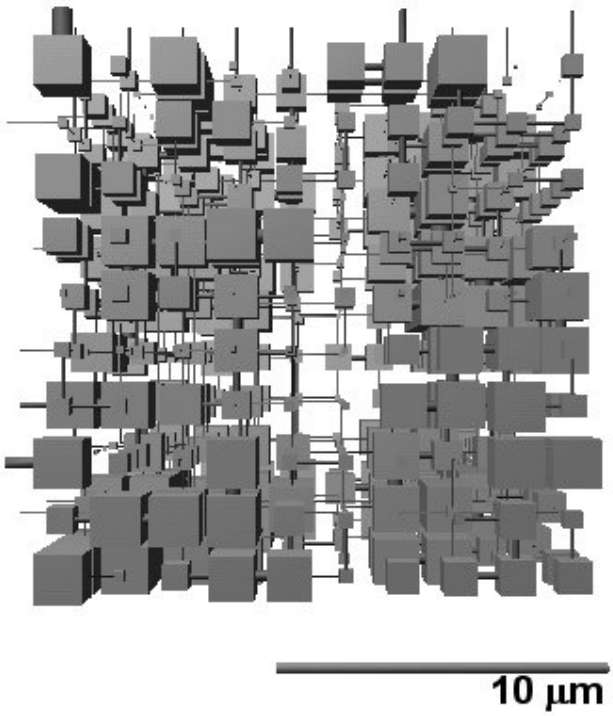

Figure 14 - Modelled structure of a low T_g latex-based coating applied with rod 2 - note the regions of small pore size illustrating the close packing and filling of pores by the deformation of the latex between the pigment particles**.**

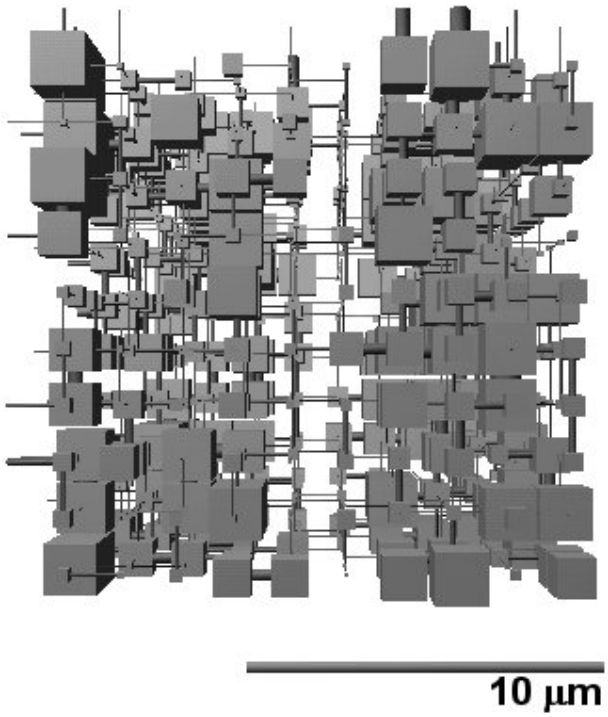

Figure 15 - Modelled structure of a low T_g latex-based coating applied with rod 3 - similarly to Fig. 14, the pore structure becomes even tighter with many very small diameter throats between the major pores.

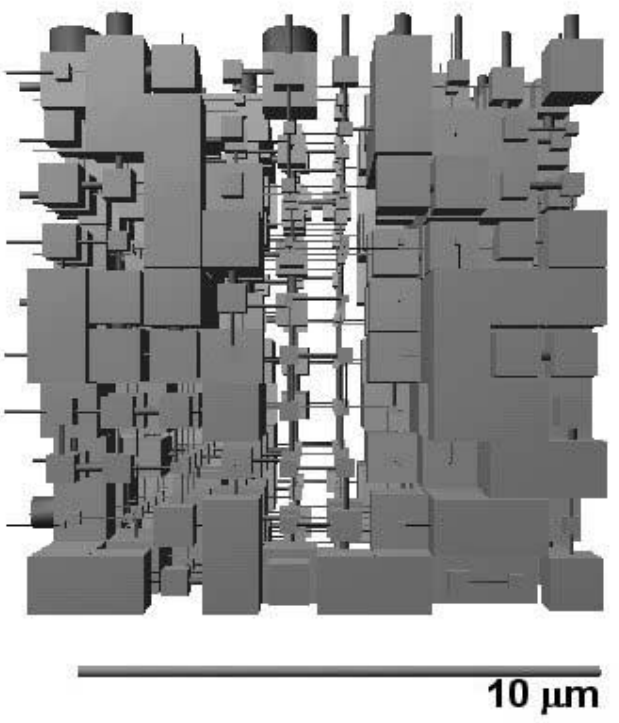

Figure 16 - Modelled structure of a high T_g latex-based coating applied with rod 2 - here the picture is different with large pores retained in the coating illustrating the resistance to shrinkage.

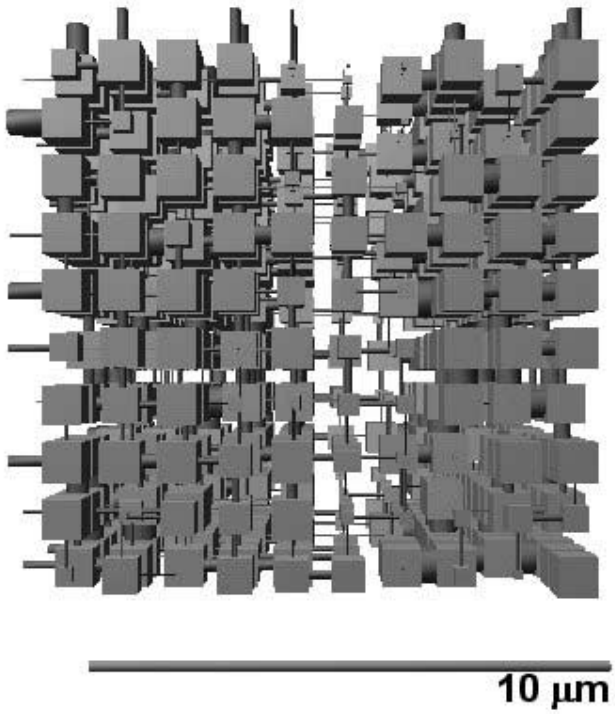

Figure 17 -Modelled structure of a high T_g latex-based coating applied with rod 3 - here we see the extra freedom of movement of the particles in the thicker layer allowing for a very uniform structure to be developed whilst resisting shrinkage.

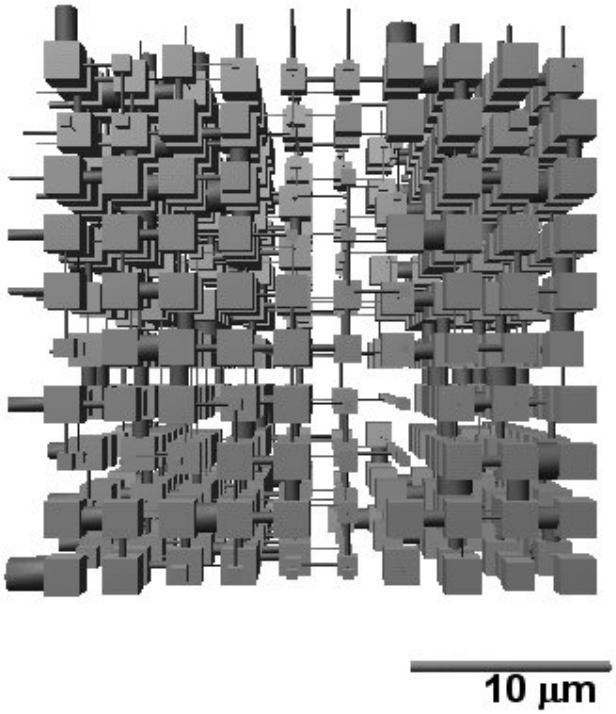

Figure 18 - Modelled structure of starch-based coating applied with rod 2 - in this case the pores are still uniform. This illustrates the formation of larger skeletal particle size in the form of flocs.

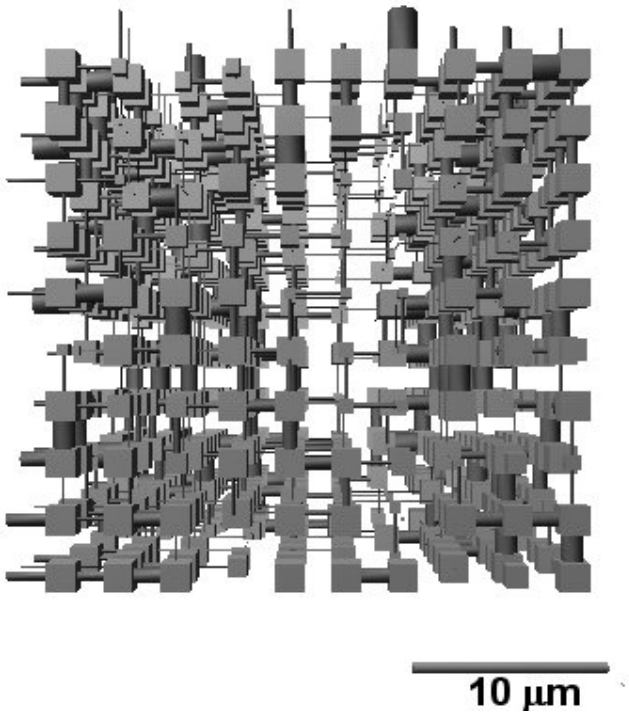

Figure 19 - Modelled structure of a starch-based coating applied with rod 3 - here we see the added effect of freedom to move in the thicker applied layer - note the smaller pores. Some of the throats are completely cut off whereas others remain large, typical of a mobile binder, and the skeletal particle size is large.

Another interesting value that the software package enables us to calculate is the particle size distribution of the skeletal material, where the particles are approximated as spherical. These results are presented in Table.2.

Table 2 – particle size distribution of the skeletal material from the modelling software

	Sample					
	High T_g latex rod 2	High T_g latex rod 3	Low T_g latex rod 2	Low T_g latex rod 3	Starch rod 2	Starch rod 3
Minimum particle size / μm	0.30	1.14	1.63	1.45	3.15	3.38
Maximum particle size / μm	1.18	1.37	2.15	1.97	3.59	3.67

DISCUSSION

The stress caused by the drying in the high T_g latex-based coating colour was less then any other sample analysed: even the control experiment, with calcium carbonate slurry only, showed more initial stress. This seems to suggest that the high T_g latex binder particles occlude the void structure. However, the latex spheres are below their T_g and minimum film-forming temperatures, so they largely maintain their shape which thus maintains the structure of the occluded coating layer. Therefore, the maximum stress, τ_{max}, is relatively low, and the strips did not retain much stress, confirming that the polymer was not filming during the air drying process at room temperature.

The experimental mercury intrusion curves seem to support the interpretation for the high T_g latex-based samples: the latex spherical particles have a diameter of 0.15 μm, as stated by the manufacturer. The mercury porosimetry experimental data show intrusion of mercury for pressures corresponding to such a value of pore-size. This supports the fact that the latex particles occlude the void structure formed by the mineral pigment particles and, being below their film-formation temperature, they do not allow the structure to deform under the action of the surface capillary forces. The FCC and SCC structures are therefore relatively similar. High values of porosity, experimentally measured, and smaller particle size distribution, calculated by the software model, seem to support the idea that particles of this latex do not film during the drying process used, leading to the formation of a structure with higher overall porosity. However, the micrographs (Fig.5 and Fig. 6) suggest that there is some partial film-forming, and surface-cracking, after the drying has been completed. This effective filming is then probably related to soluble chemical species in the latex serum, like monomers or oligomers of the latex, and liquid phase of the carbonate slurry, which are able to migrate to the surface of the coating layer and not because the latex is raised above its glass transition. The values of bulk porosity measured for the high T_g based coatings tend to confirm this interpretation.

The first part of the drying process, in the case of low T_g latex-based coating colours, is seen to be similar to the case of higher T_g. However, when the FCC has been reached, the latex particles, which are above their minimum film-forming temperature, begin to deform. Being more compressible than the high T_g latex particles, they allow the deformation of the coating layer and hence bending of the substrate to take place under the action of the surface capillary forces. The particle size distribution calculated by the network simulator shows the action of the filming-latex, with perhaps some slight pre-structuring, which leads to somewhat bigger particle agglomeration. The FCC and SCC structures in this case are therefore relatively different (further apart in terms of porosity) when compared with the high T_g case. This gives an interpretation for the values of stress acting on the surface of the strips during drying, i.e. the measured values are higher than those measured in the case of the control experiment with calcium carbonate slurry only, but this is not necessarily caused by the shrinkage of the polymeric binder itself upon drying, rather by the difference between FCC and SCC structures. The shrinkage process is free to act for a longer time and with greater spatial movement of the pigment particles together before the structure is *locked*, due to the film-formation and compressibility of the binding system, reaching higher values of stress acting on the surface. Once the structure has reached the SCC, the stress acting on the surface of the substrate is retained by the bonding effect of the latex. The values of τ measured for the two different coating weights applied support once more such an hypothesis: in the case of higher applied coating weight and, therefore, higher thickness of the coating layer, the rearrangement of the particles under the capillary forces has more freedom and not so influenced by the size of the particles in relation to the coating thickness, while in the case of a thinner coating layer the maximum diameter of the mineral pigment particles, ~ 5 μm, is very close to

the thickness of the layer, not allowing the free rearrangement of the structure in the *x* direction due to constraints in the *z* direction. When the structure is free to rearrange, the surface forces act freely for longer and the final dry structures show a lower value of porosity.

The results of the stress measurements for the samples coated using the starch coating colour formulation are far larger than in the case of the latex–based systems, but the behaviour of starch-based coating colours can be explained using the same principle. Partial adsorption of the starch [22,23] on the pigment particles and/or the depletion effect [24] cause a flocculation of the pigment particles, producing an open, loosely packing structure as groups of flocs touch one another. The lack of close-packing reduces the effective number of fine capillary-like voids in the drying coating at the initial FCC. However, once the surface menisci form, the loose floc packing at FCC transforms to the tighter SCC packing as shown by lower measured values of dry porosity, while the effective size of the particles constituting the skeletal material that is present are themselves large. The change in dimension from loose to tight packing in this system is large and so the measured stress is high, implying a high shrinkage force. The results presented in Table 2, representing the simulated particle size distribution, confirm that the skeletal particles are larger in the case of the starch-based coating colour. This is also confirmed by the micrographs in Figs. 3-8. This flocculation effect caused by the soluble natural binder is, therefore, the main cause of the higher values of τ measured for starch-based samples, i.e. the formation of flocs exists or starts in the early stages of the drying process as the system reaches the FCC. It then begins to shrink due to the capillary forces, effectively earlier in the drying process as measured by moisture than in latex-based systems. Such shrinkage is far larger for thicker coating layers due to the freedom of rearrangement of the flocs, which cannot move so freely when the layer is thinner because the floc size is close to or bigger than the thickness of the layer itself and does not allow rearrangement in the plane parallel to the free surface. This freedom of rearrangement and collapse of the floc structure between FCC and SCC result in high shrinkage stresses.

The use of pure binder systems as control confirmed that there is no measurable shrinkage of a 100 % latex layer in the systems we used. Even a 100 % starch coating layer showed only very small shrinkage, confirming that the shrinkage of the polymer upon film-forming is not the cause of the high values of surface stress measured upon drying of a starch-based coating colour formulation.

The cracking of the coating layer upon drying, which was described in the previous sections, can be explained as a discontinuous or catastrophic relief of shrinkage stress, i.e. the retreating menisci create so much stress that, due to the incompressibility of the particle packing, it can no longer be dissipated by movement in the coating, leading to the appearance of cracks.

CONCLUSIONS AND FUTURE RESEARCH

In this paper we indirectly quantified the force acting during drying, and the relative importance of capillary forces and film-forming polymer shrinkage forces.

The different behaviour of latex and starch has been analysed and quantified, showing that shrinkage in starch-based formulations causes stresses far higher than those occurring in latex-based formulations. The mercury porosimetry analysis and the software simulation on the dried porous structures, formed by the pigment and the binder, showed distinct trends, enabling us to provide potential explanations for the difference in behaviour for the different binders. The results collected experimentally and from the simulation made it possible to explain the shrinking behaviour of coatings, and the action of natural binder systems in particular, in terms of binder particle deformation in the case of low T_g latex under the action of surface capillary forces, and flocculation and collapse of the resulting loose FCC structure under the action of the ensuing capillary forces, respectively, rather than as a result of the shrinking of the polymer itself or its interaction on the pigments directly upon drying.

The importance of the freedom of rearrangement of the particles, and the limiting effect of the coating layer's thickness to such freedom has been analysed. Microscopic cracking of the coating must also be considered under these limiting conditions resulting from the very high stresses between regions of rigidly locked particles.

The next step of this research will be to start from the experimental and simulated data for the dry structures at the SCC and to calculate the network structure representing the particles' arrangement at the FCC, when the shrinkage forces start acting at the surface of the drying coating layer, and model such forces during the whole drying process.

ACKNOWLEDGEMENTS

The authors wish to thank Dr Cathy Ridgway and Dr Joachim Schoelkopf of Omya AG for their help in the instrumental development of this research project and Paul Bodurtha of the University of Plymouth for his assistance in developing the Pore-Cor model for correlated structures.

References

1. Watanabe, J., and Lepoutre, P., "A Mechanism for the Consolidation of the Structure of Clay-Latex Coatings", Journal of Applied Polymer Science, 27 pp. 4207-4219(1982).

2. Groves, R., Matthews, G. P., Heap, J., McInnes, M. D, Penson, J. E., and Ridgway, C. J., "Binder migration in paper coatings - a new perspective", Proceedings of the 12th Fundamental Research Symposium, Science of Papermaking, pp. 1149-1182(2001).

3. Pan, S. X., Davis, H. T., and Scriven, L. E., "Modeling moisture distribution and binder migration in drying paper coatings", Tappi Journal, 78(8), pp. 127-143(1995).

4. Bernada, P., and Bruneau, D., "Modeling binder migration during drying of a paper coating", Tappi Journal, 79(9), pp. 130-143(1996).

5. Bernada, P., and Bruneau, D., "Drying of a paper coating: Experimental Study and Modelling", Drying Technology, 15(9), pp. 2061-2087(1997).

6. Perera, D. Y., "Stress Phenomena in Organic Coatings," Paint and Coating Testing Manual, ASTM Manual series, edited by J. V. Koleske, pp. 585-599(1995).

7. Schoelkopf, J., Ridgway, C. J., Gane, P. A. C., Matthews, G. P., and Spielmann, D. C, "Measurement and network modelling of liquid permeation into compacted mineral blocks", Journal of Colloid and Interface Science, 227(1), pp. 119-131(2000).

8. Husband, J. C., "The adsorption of starch derivatives onto kaolin", Colloids and Surfaces, A131 pp. 145-159(1998).

9. Groves, R., and Lanham, A., "Some influences of latex on coating structure", Paper Technology, 32(1), pp. 28-34(1991).

10. Husband, J. C., "Interactions between ground calcium carbonate pigments and polymer latices", Nordic Pulp & Paper Research Journal, 15(5), pp. 382-386(2000).

11. Ridgway, C. J., and Gane, P. A. C., "Bulk density measurement and coating porosity calculations for coated paper samples", Nordic Pulp & Paper Research Journal, in press (2003).

12. Gane, P. A. C., Kettle, J. P., Matthews, G. P., and Ridgway, C. J., "Void Space Structure of Compressible Polymer Spheres and Consolidated Calcium Carbonate Paper-Coating Formulations", Industrial and Engineering Chemistry Research, 35(5), pp. 1753-1764(1995).

13. Kettle, J. P., and Matthews, G. P., "Computer Modelling of the Pore Structure and Permeability of Pigmented Coatings," proceeding of the 1993 Tappi Advanced Coating Fundamentals Symposium, Tappi Press, Atlanta, pp. 121-126(1993).

14. Matthews, G. P., and Ridgway, C. J., "Pore-Cor - a 3-dimensional approach to study Porosity from

Mercury Porosimetry Curves", Fourth Micromeritics Particle Technology Workshop, Veldhoven, Belgium (1997).

15. Matthews, G. P., Moss, A. K., Spearing, M. C., and Voland, F., "Network Calculation of Mercury Intrusion and Absolute Permeability in Sandstone and Other Porous Media", Powder Technology, 76(1), pp. 95-107(1993).

16. Bodurtha, P., Matthews, G. P., Kettle, J. P., Lohmander, S., and James, P. W., "The influence of structural anisotropy on fluid permeation in porous media", proceeding of the 2001 Tappi Advanced Coating Fundamentals Symposium, Tappi Press, San Diego, California, pp. 393-438(2001).

17. Matthews, G. P., Ridgway, C. J., and Small, J. S., "Modelling of simulated clay precipitation within reservoir sandstones", Marine and Petroleum Geology, 13(5), pp. 581-589(1996).

18. Ridgway, C. J., and Gane, P. A. C., "Dynamic Absorption into Simulated Porous Structures", Colloids and Surfaces A-Physicochemical and Engineering Aspects, 206 pp. 217-239(2002).

19. Schoelkopf, J., Gane, P. A. C., Ridgway, C. J., and Matthews, G. P., "Influence of Inertia on Liquid Absorption into Paper Coating Structures", Nordic Pulp and Paper Research Journal, 15(5), pp. 422-430(2001).

20. Schoelkopf, J., Gane, P. A. C., Ridgway, C. J., and Matthews, G. P., "Practical observation of deviation from Lucas-Washburn scaling in porous media", Colloids and Surfaces A-Physicochemical and Engineering Aspects, 206 pp. 445-454(2002).

21. Xiang, Y., and Bousfield, D., "Effect of Coat Weight and Drying Condition on Coating Structure and Ink-Setting," proceeding of the 2001 Tappi Advanced Coating Fundamentals Symposium, TAPPI Press, San Diego, California, pp. 35-46(2001).

22. Järnström, L., Lason, L., and Rigdahl, M., "Flocculation in kaolin suspensions induced by modified starches 1. Cationically modified starch - effects of temperature and ionic strength", Colloids and Surfaces A-Physicochemical and Engineering Aspects, 104 pp. 191-205(1995).

23. Järnström, L., Lason, L., Rigdahl, M., and Eriksson, U., "Flocculation in kaolin suspensions induced by modified starches 2. Oxidized and hydrophobically modified oxidized starch in comparison with poly (vinyl alcohol) and carboxymethylcellulose", Colloids and Surfaces A-Physicochemical and Engineering Aspects, 104 pp. 207-216(1995).

24. Yan, Y. D., Burns, J. L., Jameson, G. J., and Biggs, S., "The structure and strength of depletion force induced particle aggregates", Chemical Engineering Journal, 80 pp. 23-30(2000).